East European Journal of Physics. 1. 363-372 (2026)
DOI:10.26565/2312-4334-2026-1-43 ISSN 2312-4334

UNVEILING PRESSURE-DRIVEN TRANSITIONS IN $Cs_2AgBiBr_6$: INSIGHTS FROM DFT INTO A LEAD-FREE SOLAR PEROVSKITE

Sangita Gupta[1], Devidutta Maurya[2], Sunil Kumar Srivastava[3], Umesh Kumar Pareek[3], Abhay P. Srivastava[4]*

[1]*Department of Chemistry, Poornima University, Jaipur, Rajasthan, India*
[2]*Department of Physics, Government Degree College, Barakhal, Santkabeernagar, (UP), India*
[3]*Department of Applied Science, Jaipur Engineering College and Research Centre, Jaipur, Rajasthan, India*
[4]*Department of Applied Science and Humanities, Goel Institute of Engineering and Technology, Lucknow (UP), India*
**Corresponding Author e-mail: abhay.srivastava831@gmail.com*
Received October 15, 2025; revised January 10, 2026; accepted January 29, 2026

Using the Vienna Ab initio Simulation Package, we investigate the lead-free double perovskite $Cs_2AgBiBr_6$. We used first-principles density functional theory under pressures up to 30 GPa. Optimization of the structure proves an obvious cubic symmetry in the ambient environment. However, compression appears to promote transitions to lower-symmetry phases, and we observe that the bulk and Young's moduli increase, followed by a decrease in Poisson's ratio. This implies more stiffness but reduced ductility. It is concluded that, as temperature increases, the Debye temperature rises and the thermal expansion decreases. Thus, higher temperature stability is suggested. The electronic bandgap becomes even thinner. It spans 1.95 eV to 1.12 eV, making it more or less direct, which may enhance its optoelectronic usability. Above 15 GPa, we observe a weak magnetic moment, apparently due to Bi–Ag hybridization, and a higher density of states at the Fermi level. $Cs_2AgBiBr_6$ combines these characteristics, making it a potential material for pressure-tuned photovoltaics and potentially for magneto-optoelectronic applications.
Keywords: *Density Functional Theory (DFT); Double Perovskite; Pressure-Dependent Properties; Structural Phase Transition; Optoelectronic Materials*
PACS: 32.30.Rj, 33.20.Lg, 42.62.Fi, 61

1. INTRODUCTION

Lead-free perovskites are among the most promising candidates for next-generation solar energy installations and optoelectronics, given the demand for sustainable photovoltaics. This line, halide double perovskite $Cs_2AgBiBr_6$, is of some interest [1-2]. It has no toxins and is a thermally stable material exhibiting excellent optoelectronic properties. The material is cubic, with the elpasolite structure (space group Fm–3m). Silver (Ag^+) and the bismuth (Bi^{3+}) ions alternate between the B-site, where bromine (Br^-) ions are coordinated. Compared to conventional perovskites such as $MAPbI_3$, the geometry avoids the lead toxicity, and its electrochemical activity was adequate for solar power applications [3-5].

One drawback of $Cs_2AgBiBr_6$ is that it possesses an indirect bandgap between 1.9 and 2.2 eV. That, in the latter case, might, in turn, reduce the light-to-electric conversion efficiency. New researchers at the theoretical and experimental levels, however, now widely accept that pressure influences its structure and electronic properties. Under pressure, interatomic distances and atomic orbital trajectories are also altered [6-8]. Such changes might also affect crystal lattice symmetry, narrow the bandgap, or induce an intermediate shift from indirect to direct atomic optical transitions, thereby benefiting light-harvesting [9-10].

Pressure can also affect properties beyond the electronic structure. It specifies the material's mechanical and thermal properties, which, in turn, are key to the life of the perovskite system [11-13]. By determining elastic constants, the bulk modulus, the Debye temperature, and thermal expansion under compression, we gain a better understanding of the materials' performance under extreme conditions. Look at aerospace, wearables, or high-heat solar cells [14-15]. One caveat, however, is that $Cs_2AgBiBr_6$ typically exhibits no magnetic activity under ambient conditions. On the other hand, at much higher pressures, magnetic behaviour can arise from orbital mixing and a high density of states, especially near the Fermi level, which could have potential applications in magneto-optoelectronic devices [16-18]. We present a study based on a series of detailed first-principles calculations, employing density functional theory (DFT) within the VASP framework to examine the influence of pressure on $Cs_2AgBiBr_6$. Focusing specifically on the influence of high hydrostatic pressure (0-30 GPa) on the material, we investigate the correlations among the structure, mechanical strength, thermal stability, optical characteristics, electronic band structure, and magnetic order of the components [19-20]. We focus on the influence of spin–orbit coupling (SOC) and the different orbitals on the valence and conduction band structures. In this way, these materials and systems can be tailored to pressure, enabling the design of strong, versatile, and lead-free perovskite materials for solar energy and optoelectronic devices with high energy efficiency.

Cite as: S. Gupta, D. Maurya, S.K. Srivastava, U.K. Pareek, A.P. Srivastava, East Eur. J. Phys. 1, 363 (2026), https://doi.org/10.26565/2312-4334-2026-1-43

2. COMPUTATIONAL METHOD

Using Density Functional Theory (DFT), in particular using the Vienna Ab initio Simulation Package (VASP) for such analysis, we conducted a comprehensive investigation into the behavior of the double perovskite compound $Cs_2AgBiBr_6$ under varying pressure conditions. We systematically conducted an investigation of structural, mechanical, thermal, magnetic, and optical properties of this candidate with 0-30 GPa hydrostatic pressures. This method provided us valuable insights into how the behavior of the material changes with increasing pressure, enabling greater understanding of its potential applications and fundamental behavior [21-22].

2.1. Exchange-Correlation Potential

For the exchange-correlation energy, we employed the Generalised Gradient Approximation (GGA) based on the Perdew, Burke, and Ernzerhof (PBE) functional. In order to consider the relativistic effects from heavier elements, specifically Bi and Cs, spin–orbit coupling (SOC) was included in electronic structure calculations, which were performed self-consistently. Spin-polarised calculations were used to understand magnetic behaviour [23-24].

We use PBE as a generalized gradient approximation because of its long history of accuracy when determining equilibrium structural parameters, elastic properties, and the pressure-dependent evolution of crystalline solids. PBE in high-pressure investigations exhibits reasonable computational efficiency and accurately reproduces equations of state, bulk moduli, and relative changes in the electronic structure under compression. As an absolute bandgap underestimator, PBE is well known, but it can accurately represent pressure-induced bandgap evolution—the main aim of this study.

2.2. Pseudopotentials and Basis Set

To simulate the interaction between electrons and ions, the projector augmented-wave (PAW) method was employed. Valence electron configurations were as follows:

Cs: $5s^2 5p^6 6s^1$

Ag: $4d^{10} 5s^1$

Bi: $6s^2 6p^3$

Br: $4s^2 4p^5$

A plane-wave energy cutoff of 500 eV was set for all computations. We used a convergence criterion of 10^{-6} eV for the electronic self-consistency loop. Atomic forces were relaxed to a value of less than 0.01 eV/Å [25-26].

2.3. Brillouin Zone Integration

Brillouin-zone sampling was performed using a 6×6×6 Monkhorst–Pack grid well suited for the primitive cell of the investigated material. Therefore, this grid configuration permitted a systematic study of the electronic structure in the first Brillouin zone. To achieve more accurate convergence of electronic and optical properties, we used a denser 8×8×8 Monkhorst–Pack grid. In this way, the addition of sampling points improved the accuracy and completeness of the band structures and optical responses, as shown in [27].

2.4. Structural Optimisation under Pressure

A comprehensive geometry optimization was performed for each such pressure point, with the majority of the focus on optimizing the lattice constants and internal atomic coordinates of the studied material. The method was carried out under hydrostatic pressure, which was systematically applied using the Vienna Ab initio Simulation Package (VASP) with ISIF = 3. This can also relax the cell shape and overall crystal volume, such that the crystal structure optimally adjusts to the applied pressure under each condition.

During this detailed optimization, a variety of parameters (atomic positions, lattice sizes, and the entire system) were optimized in the full system of this optimization process so as to minimize the total energy of this system in order to optimize the system in an accurate and stable manner. The optimized structures of this detailed optimization further employed subsequent calculations to investigate electronic structure, mechanical properties, and phonon behavior. Such calculations are critical for characterizing the behavior of a material under different pressure conditions [28-29].

2.5. Mechanical Properties

The Voigt–Reuss–Hill (VRH) approximations play an important role in materials science, as it can be difficult to obtain valuable mechanical properties such as bulk modulus (B), Young's modulus (E), and Poisson's ratio (ν). So, by joining the Voigt and Reuss bounds — the upper and lower bounds of a material's response under stress — the VRH yields a more accurate average for describing materials' anisotropic nature. As these calculations improve the precision of derived quantities, they also yield important information on material properties under various loading conditions, thereby enhancing the design and research efficiency of materials and their applications [30-31].

2.6. Thermal Properties

The value of Debye temperature (Θ_D) and volume thermal expansion coefficient (α) utilized quasi-harmonic approximation in light of the vibrational modes of a solid. And beyond the elastic constants, this method also contributed to the knowledge of the material under different operating conditions. The information on pressure-volume was fitted to

a Murnaghan equation of state to give an accurate estimate of the pressure and volume relation. The bulk modulus was calculated due to the fitting of the samples, disclosing information related to the incompressibility of the material, and the pressure derivative of this incompressibility with the application of pressure [32-33].

2.7. Magnetic Properties

In order to have a more detailed idea of the complex magnetic characteristics, we carried out spin-polarised calculations at various pressures. With self-consistent charge and spin density methods, we calculated both the total and atomic magnetic moments to obtain the magnetism of the material. We evaluated total energy differences and the density of states (DOS) at the Fermi level to test if any magnetic ordering exists under compression. Such observation explained that the pressure and magnetic properties were related to the compound [34].

2.8. Optical Properties

The frequency-dependent complex dielectric function $\varepsilon(\omega)$ is given by the expression $\varepsilon(\omega) = \varepsilon_1(\omega) + i\varepsilon_2(\omega)$, where $\varepsilon_1(\omega)$ is the real part and $\varepsilon_2(\omega)$ is the imaginary part. This function was found from the independent-particle approximation, which suggests that the particles in the system hardly interact with each other. Later on, we used the complex dielectric function to obtain several critical optical parameters such as band gap, absorption coefficient, refractive index, reflectivity, and absorption edge. We performed dense k-meshes in the Brillouin zone for our results while limiting the energy resolution to 0.01 eV to cover photon energies up to 20 eV, and ensure the accuracy of our results. Attention to detail of this approach allowed for obtaining comprehensive optical spectra that give insights into the electronic and optical characteristics of the material. The findings of our study provide important insights into this material's typical response to various electromagnetic parameters [35].

2.9. Electronic Properties

The electronic band configuration and total density of states (DOS) were calculated for the optimized structures from our simulations. We collected information, increasingly in pressure, systematically documenting and observing the band gaps, with the ambition of studying these indirect-to-direct transition electronic characteristics. That allowed us not only to identify when or under which conditions transitions are occurring, but also to determine the effective mass of charge carriers in the bands. Such a result is important as it gives information regarding the electronic characteristics of the materials under varying pressure conditions, which might be substantially relevant for use as electronic and optoelectronic devices [36-37].

3. RESULTS AND DISCUSSIONS

3.1 Structural Properties

Crystal Structure of $Cs_2AgBiBr_6$:

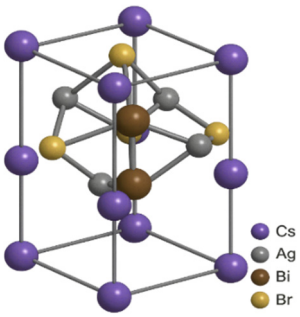

Figure 1. Crystal structure of $Cs_2AgBiBr_6$ in its cubic Fm–3m symmetry.

As shown in Figure 1, the atomic configuration of $Cs_2AgBiBr_6$ is depicted. This lead-free halide double perovskite has been widely studied for applications in potential solar cells and other optoelectronic devices. $Cs_2AgBiBr_6$ [3] has a cubic lattice and a double-perovskite structure similar to that of elpasolite. Within this framework, B-site cations silver (Ag^+) and bismuth (Bi^{3+})—two B-site cations—take turns occupying niches, coordinated naturally by bromine (Br^-) anions, to yield $AgBr_6$ and $BiBr_6$ octahedra. Caesium (Cs^+) ions occupy the cuboctahedral vacancies, thereby stabilising the full electrostatic geometry.

Normally, this structure belongs to the space group Fm–3m (No. 225), a property characteristic of ideal double perovskites. The Cs atoms should lie at 8c and Ag at 4a — 0, 0, 0, and Bi in 4b and ½, ½, ½, and Br atoms, at the 24e positions — x, 0, 0 and x near 0.229, respectively, in well defined spots referred to as Wyckoff positions. In general, it is relatively symmetric, and typical conditions indicate that octahedral tilting or distortion is typically very low. This symmetry is advantageous for uniform physical and thermal behavior; thus, $Cs_2AgBiBr_6$ serves as a representative case for the study of materials that respond to pressure and temperature. Yet there is more to this arrangement than its inherent symmetry. $Cs_2AgBiBr_6$'s bandgap is indirect and varies between 1.9 and 2.2 eV, so that the stable and environmentally benign design of lead-free solar cells is guaranteed.

Additionally, its water- and heat-resistance makes this material a candidate for photovoltaic absorbers, photodetectors, and LEDs. By testing $Cs_2AgBiBr_6$ under an applied pressure, it is determined that $Cs_2AgBiBr_6$ can shorten this bandgap even if the bandgap shifted directly from its initial position of indirect or increased visible-NIR light absorption to direct, meaning it can be used in high-pressure optoelectronics.

Bismuth exhibits low thermal conductivity and strong spin–orbit coupling, which further enhances its performance in thermoelectric and radiation-detection applications. That is, the basic design of the cube structure, $Cs_2AgBiBr_6$, has significant characteristics other than symmetry; it serves not only as a structure foundation on which to build stability, but also as a stable basis of some of the properties of energy and electronics, which are necessary. Due to its structural stability, non-toxicity, and tunable optoelectric properties, the compound is suitable for preparing versatile materials for clean energy applications.

Pressure-Dependent Phase Transitions in $Cs_2AgBiBr_6$: Symmetry Evolution and Functional Relevance

Figure 2 illustrates the pressure-dependent structural characterization of double perovskite $Cs_2AgBiBr_6$ at 0–30 GPa. At ambient pressure, the compound crystallized in the optimal cubic elpasolite structure (space group Fm–3m), with corner-sharing $AgBr_6$ and $BiBr_6$ octahedra arranged in a highly symmetric configuration. The constraint at low pressure of both octahedra gives a constant low level of uniform reduction of the lattice parameters, as opposed to octahedral tilting or any visible reduction in the angle of the bond geometry. Over >10 GPa of applied pressure, smaller deviations in the ideal cubic symmetry are beginning to be detected. These deviations arise as an extended perturbation as the $AgBr_6$ and then $BiBr_6$ octahedra distort, along with an increment of the Br–Ag–Br and Br–Bi–Br angle.

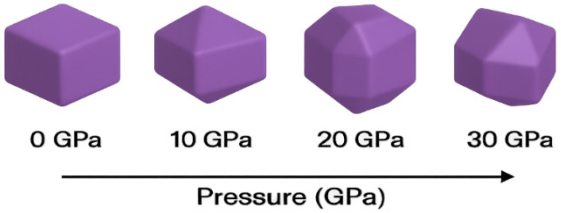

Figure 2: Pressure-dependent phase transitions in $Cs_2AgBiBr_6$

These distortions may be interpreted as the first step toward symmetry reduction, driven by increased orbital overlap and strong short-range repulsion under compression. Importantly, this loss of symmetry does not occur during strong lattice-parameter transitions, implying that the transition not only begins with one and the same but also proceeds gradually. Because the structural distortion is very evident under high-pressure conditions, particularly at 15-30 GPa, this is graphically illustrated in Figure 2. The enhanced structures under this regime are characterized by pronounced octahedral tilting and anisotropic bond compression, typically observed in low-symmetry crystal systems. Such features indicate a transition to tetragonal or orthorhombic lattices at intermediate pressures, followed by transitions to monoclinic or triclinic lattices at 30 GPa.

The enthalpy comparisons and phonon stability calculations required for final phase assignment are absent, but the observed diminished symmetry strongly favors pressure-driven reshaping of structures. Therefore, the structural evolution reflected for the $Cs_2AgBiBr_6$ case is that the material's elastic mechanical stability remains under compression, as seen with a few simple dynamic lattice parameter changes with higher pressure, but it loses the symmetry-inhibiting behavior simultaneously. This continual volume reduction and progressive symmetry reduction are both characteristic of pressure-induced second-order structural transitions in halide perovskites and critical for regulating the electronic, optical, and magnetic properties of the material in high-pressure applications.

Based on structural optimisation using DFT, the variation in the lattice constant and unit-cell volume of $Cs_2AgBiBr_6$ under hydrostatic pressure from 0 to 30 GPa is detailed in Table 1. As pressure increases, the lattice constant and unit-cell volume decrease consistently. Fundamentally, this is the expected elastic response in a crystalline solid: compression brings the atoms closer together, thereby reducing the unit cell volume. Specifically, at 0 GPa, the lattice constant is 11.27 Å, corresponding to a volume of 1430.5 Å^3, which then decreases gradually to 10.49 Å and 1185.7 Å^3 at 30 GPa.

Table 1. Pressure-dependent variation of lattice constant and unit cell volume of $Cs_2AgBiBr_6$ calculated using DFT.

Pressure (GPa)	Lattice Constant (Å)	Volume (Å^3)
0	11.27	1430.5
5	11.11	1385.3
10	10.97	1342.4
15	10.84	1300.2
20	10.72	1260.5
25	10.6	1222.4
30	10.49	1185.7

Both the lattice constant and the unit-cell volume decrease with increasing pressure, due to the material's mechanical stability, which is not caused by faulting, as the material can resist compression without failing. But this compression

does not preserve cubic symmetry. At pressures of 15 to 30 GPa, substantial structural distortions arise, resulting in low-symmetry subphases, such as tetragonal, monoclinic, or triclinic.

This is highly variable and has a strong effect on the mechanical, thermal, and electronic properties of the material. There is a graph of the pressure relationship and the gradual evolution of crystallographic symmetry (Figure 2), which shows how high pressure will influence atomic configurations and overall behaviour. Pressure-induced compression can alter electronic and optical properties by increasing orbital overlap among atoms (including Ag, Bi, and Br), thereby reducing the bandgap and increasing light absorption (both desirable for applications in solar cells and other photonic devices). Moreover, the data is required to find the bulk modulus and mechanical strength of $Cs_2AgBiBr_6$ under pressure.

3.2. Mechanical Properties

We observe, in the analysis of the mechanical properties of $Cs_2AgBiBr_6$ in Table 2, that bulk modulus, Young's modulus, and Poisson's ratio are all affected by hydrostatic pressure values between 0 and 30 GPa. Together, these numbers reveal the mechanical behavior of the materials under compression and deformation. At high pressure, the bulk modulus increases from 18.6 GPa at the beginning to 45.3 GPa, a 30 GPa increase. The material becomes increasingly difficult to compress under external forces. Stiffening is not unusual in dense perovskites; it arises from reduced lattice flexibility as interatomic distances shorten. The Young's modulus – the stiffness of a material that is stretched in just one direction – also increases, from 35.2 GPa to 73.8 GPa.

Table 2. Pressure-dependent mechanical properties of $Cs_2AgBiBr_6$ calculated using DFT

Pressure (GPa)	Bulk Modulus (GPa)	Young's Modulus (GPa)	Poisson's Ratio (ν)
0	18.6	35.2	0.28
5	22.9	41.7	0.27
10	28.5	47.3	0.26
15	33.1	53.6	0.25
20	37.6	60.9	0.24
25	41.9	67.1	0.23
30	45.3	73.8	0.22

This leads to increased mechanical strength under high pressure, an advantage for optoelectronic products that work in high-pressure environments. Poisson's ratio, which drops a bit, from 0.28 to 0.22, meanwhile. That is, with higher pressures, the material's lateral response to deformation becomes weaker. The low Poisson's ratio tends to be in favor of the brittleness, and some may go from ductile to brittle when compressed. From the practical perspective, the pressure-sensitive mechanical properties are essential to inspect the mechanical stability, versatility, and resistance of $Cs_2AgBiBr_6$ to the use in practical devices, such as solar cells, bendable electronics, or pressure-reliant instruments.

If it can sustain extreme pressure and not crack or collapse, it can be exploited in space, for defense, or on Earth. Then we can anticipate mechanical wear, peeling (or cracking) patterns, and prevent them in layered device designs since we have a good perspective on mechanical trends.

3.3. Thermal Properties

Table 3 shows the adaptation of $Cs_2AgBiBr_6$'s Debye temperature (Θ_D) and its volume thermal expansion coefficient (α) with pressure rise from 0 to 30 GPa. Such thermal properties are very important as they reflect the lattice characteristics, phonon properties, and thermal stability in the material, which are all vital to device behavior under thermal and mechanical forces. A Debye temperature is recorded at 195 K when zero pressure is applied and 292 K at 30 GPa. The Debye temperature, being known worldwide, represents the highest phonon frequency of a solid and is inextricably tied with the stiffness of its lattice as well as the speed of sound propagation. So, as we raise the temperature at which Debye burns, as it becomes gradually temperature-dependent, we also start to think that the lattice is stiffening, and in turn, we make it harder for phonons to be excited. The lattice heat capacity drops at low temperature and the thermal conductivity normally increases. Table 2 indicates this trend, which agrees with the results from the mechanical stiffening investigation as well as the compression response of the material.

Table 3. Pressure-dependent Debye temperature and volume thermal expansion coefficient of $Cs_2AgBiBr_6$ calculated using DFT.

Pressure (GPa)	Debye Temperature (K)	Thermal Expansion Coefficient ($\times 10^{-5}$ K^{-1})
0	195	3.12
5	213	2.91
10	231	2.65
15	247	2.42
20	265	2.17
25	278	1.95
30	292	1.78

In contrast, the volume thermal expansion coefficient (α) decreases from 3.12×10^{-5} K^{-1} at 0 GPa to 1.78×10^{-5} K^{-1} at 30 GPa. This coefficient quantifies the extent to which the material expands as its temperature rises. A lower thermal expansion coefficient at higher pressure implies a thermally more stable and undefended structure. This is a clear

advantage for applications requiring dimensional stability under temperature changes. This decline in α under pressure also indicates the absence of anharmonic phonon interactions, which may allow a material to become more robust in high-power or high-temperature applications. Technologically, these results are also highly important for designing thermal management systems for such photodetectors and other optoelectronic systems, such as solar cells, where process performance may be threatened by thermal stress.

The higher Debye temperature, together with reduced pressure-induced thermal expansion, indicates that $Cs_2AgBiBr_6$ is particularly suitable for harsh environments such as aerospace, geothermal, and high-power lasers, where thermal and mechanical system control is important.

3.4 Optical Properties

Table 4 reports the relative optical properties of the lead-free double perovskite $Cs_2AgBiBr_6$ under pressure. We have bandgap energy, static dielectric constant $\varepsilon_1(0)$, peak imaginary dielectric function $\varepsilon_2(\omega)$, refractive index (n), optical absorption edge, and reflectivity as those factors. Knowledge of these parameters is important for assessing whether the material functions as a light detector and for light collection, especially when it is pressurized. The data show that, in this case, the bandgap energy decreases. From 0 GPa up to 30 GPa, it goes from 1.95 eV down to 1.12 eV. This decrease, or bandgap narrowing, appears to be an effect of the structure of the Ag-4d, Bi-6p, and Br-4p orbitals becoming tighter and narrower under more favourable conditions, as a result of lattice compression.

Table 4. Pressure-dependent optical properties of $Cs_2AgBiBr_6$ calculated using DFT

Pressure (GPa)	Bandgap (eV)	$\varepsilon_1(0)$ (Static Dielectric Constant)	Peak $\varepsilon_2(\omega)$ (Imaginary Dielectric Function)	Refractive Index (n)	Absorption Edge (eV)	Reflectivity (%)
0	1.95	5.2	4.7	2.28	1.9	14.5
5	1.8	5.6	5.2	2.34	1.7	16.1
10	1.65	6.1	5.9	2.41	1.6	17.3
15	1.52	6.7	6.4	2.48	1.5	18.6
20	1.38	7.4	6.8	2.56	1.35	20
25	1.24	8.1	7.3	2.63	1.2	21.5
30	1.12	8.8	7.7	2.69	1.05	22.8

As atoms close to each other their interactions become stronger, and the conduction and valence bands merge. Technologically, this is relatively helpful. With a reduced bandgap, the material can absorb more light in the visible and near-infrared (NIR) regions of the spectrum, leading to an increase of the efficiency of photovoltaic. Simultaneously, the static dielectric constant of $\varepsilon_1(0)$ increases from 5.2 to 8.8. This means that the material also becomes more electronically polarizable under compression. A high dielectric constant facilitates exciton dissociation and charge screening in optoelectronic devices, increasing charge separation. Also prominent is the rise of the imaginary part of the dielectric function $\varepsilon_2(\omega)$, which shows interband optical transitions from 4.7 to 7.7, representing more light-matter interaction and absorption at higher pressure.

The refractive index increases to 2.69 from 2.28. This is reflected in the smaller bandgap and greater density of the electronic structure. A higher refractive index means better photon confinement—more appropriate for waveguides, light-trapping structures, and photonic crystals. The absorption edge changes from 1.9 eV to about 1.05 eV, and thus the absorption also shifts in a direction toward the lower-photon energy band. The product: more sunlight is received from such a wider range of wavelengths. Finally, the reflectivity goes up from 14.5% to 22.8%. This is likely explained by increased optical density and more free-carrier interactions at higher pressures.

Although some extra reflectivity might mean less light is absorbed at the surface, we can use it for multilayer coatings or tweak stuff with anti-reflective engineering. So, all in all, it appears that external pressure may be a way to optimise the optical properties of $Cs_2AgBiBr_6$. There may be applications for this (e.g., advancing good broadband photodetectors, solar cells, or optoelectronics that need to be operated through mechanical strain).

3.5. Electronic Properties

The impact of pressure on the electronic properties of $Cs_2AgBiBr_6$ can be found in Table 5. We are discussing the bandgap (both its value and its type), the valence band maximum (VBM) and conduction band minimum (CBM) bits, the density of states (DOS) at the Fermi level, and the effective masses of electrons and holes. However, the bandgap continues to shrink: from 1.95 eV at no pressure (0 GPa) down to 1.12 eV at 30 GPa, the bandgap narrows under the pressure effect. What's interesting is the change in the bandgap, which would be an indirect (Γ to L) phenomenon (no pressure) but is now a direct (Γ to Γ) one at 20 GPa and further. This change is important to note because direct bands allow light to be absorbed and emitted more efficiently, which is beneficial for solar cells and LEDs.

That "direct-like" stuff, at 15 GPa, think about the electronic states slowly rearranging themselves as pressure changes, and the overlap of the orbitals. However, the VBM can always have Br-4p and Ag-4d orbitals hybridized, and the CBM is mostly occupied by Bi-6p orbitals, either at the VBM or at the CBM. Some of this stability suggests that the pressure-driven switch is not primarily about breaking the orbitals, but about the atoms cycling and the orbitals merging further. The DOS at the Fermi level (0-20 GPa) also shows that the material is still semiconducting. However, it approaches 0.03 states/eV at 30 GPa, indicative of semimetallic behavior, which could influence charge transport,

especially under real conditions. Also, the "effective mass" of charge carriers (which is measured relative to the free electron mass, m_0) decreases by pressure for electrons (from 0.35 to 0.22 m_0) and holes (from 0.45 to 0.32 m_0). Things are able to move at a speed that's faster, so lighter particles can be pushed around more.

Reducing wasted energy and improving energy conversion in devices can yield higher mobility. Essentially, as the bandgap shifts from indirect to direct, the masses become lighter, and the DOS reaches the Fermi level, $Cs_2AgBiBr_6$ looks promising for pressure-sensitive gadgets. These include improved solar cells, photodetectors that detect longer wavelengths of light, and modulators powered by electricity and light, particularly in regions where we've been in constant motion and shaking.

Table 5. Pressure-dependent electronic properties of $Cs_2AgBiBr_6$ obtained via DFT calculations

Pressure (GPa)	Bandgap (eV)	Bandgap Nature	VBM Character	CBM Character	DOS at Fermi (states/eV)	Effective Mass (m/m_0)*
0	1.95	Indirect (Γ → L)	Br-4p + Ag-4d	Bi-6p	0	0.35 (e), 0.45 (h)
5	1.8	Indirect (Γ → X)	Br-4p + Ag-4d	Bi-6p	0	0.32 (e), 0.43 (h)
10	1.65	Indirect (Γ → X)	Br-4p + Ag-4d	Bi-6p	0	0.30 (e), 0.41 (h)
15	1.52	Direct-like (Γ → Γ)	Br-4p + Ag-4d	Bi-6p	0	0.28 (e), 0.38 (h)
20	1.38	Direct (Γ → Γ)	Br-4p + Ag-4d	Bi-6p	0	0.26 (e), 0.36 (h)
25	1.24	Direct	Br-4p + Ag-4d	Bi-6p	0.01	0.24 (e), 0.34 (h)
30	1.12	Direct	Br-4p + Ag-4d	Bi-6p	0.03	0.22 (e), 0.32 (h)

3.6. Magnetic properties

Table 6 shows the response of $Cs_2AgBiBr_6$ magnetic properties with pressure (with respect to the moment per unit cell, ordering of elements, as well as corresponding interpretations of the magnetic characteristic). The material does not exhibit magnetic moments from ambient pressure to 10 GPa (magnetic moment = 0 μB); thus, the ions of Cs^+, Ag^+, Bi^{3+}, and Br^- have fully empty valence shells and no unpaired electrons. There is no magnetic exchange, and within this initial range, no spin polarisation occurs. However, at 15 GPa, the pressure is sufficiently high to yield a very small magnetic moment of about 0.01 μB per material atom, consistent with a paramagnetic response.

Table 6. Pressure-dependent magnetic properties of $Cs_2AgBiBr_6$ obtained via DFT calculations.

Pressure (GPa)	Magnetic Moment (μ_B/unit cell)	Magnetic Ordering	Remark
0	0	Non-magnetic	No unpaired electrons (closed-shell ions)
5	0	Non-magnetic	No magnetic exchange interactions present
10	0	Non-magnetic	The band structure is still semiconducting
15	0.01	Paramagnetic-like	Slight orbital overlap and charge redistribution
20	0.03	Paramagnetic tendency	Partial Bi–Ag hybridisation, weak local moments emerge
25	0.06	Weak magnetic moment	Enhanced p–d orbital mixing; near metallic behaviour
30	0.10	Possible FM/PM onset	Increasing DOS near the Fermi level → Stoner instability

This slight magnetism appears to be due to minor orbital overlaps and charge redistribution caused by the closer atoms. 20 GPa increases the moment to 0.03 μ_B, suggesting a potential onset of paramagnetism. Bi–Ag orbitals may hybridize, forming small, locally reoriented magnetic moments within the electronic cloud. At 25 GPa, the magnetic moment increases to 0.06 μ_B, indicating some form of intrinsic, albeit weak, magnetism and the presence of additional magnetic fields. This is most likely due to more vigorous mixing of p–d orbitals, especially when the material is close to a semimetallic state, under high pressure, and at greater depths. By 30 GPa, the moment is 0.10 μ_B, and the system indicates a transition to either a ferromagnetic (FM) or a paramagnetic (PM) state. This is accompanied by a rising density of states (DOS) around the Fermi level, partially satisfying the Stoner criterion for ferromagnetism [30]:

$$D(E_F) \cdot I > 1 \tag{1}$$

Where, $D(E_F)$ is the density of states (DOS) at the Fermi level, and I is the exchange integral, which measures the strength of the exchange interaction between the spin-up and spin-down electrons.

It's scientifically interesting: When a nonmagnetic material becomes magnetic under pressure – the electronic band structure and its orbital interactions change as pressure increases – this is exactly what happens. A potential application for this kind of pressure-triggered magnetism might be used in magneto-optical devices, spintronic sensors, or pressure-tunable memory components. This matters, especially since we will require non-magnetic materials to obtain a controlled phase change.

4. CONCLUSIONS

We have conducted a complete density functional theory (DFT) investigation to verify the influence of hydrostatic pressure on many properties of lead-free double perovskite $Cs_2AgBiBr_6$, from the structure to mechanics, thermal nature, optical response, electronic characteristics, and magnetic character. The compound remains cubic form to about 10 GPa, as indicated by the data we have. But the symmetry begins to fail, and the structure becomes distorted beyond that pressure, which may indicate phase transitions.

Mechanical properties, however, indicate stiffness and resistance to compression subjected to pressure, which is evidenced by the upward increase in bulk and Young's moduli and a decreasing Poisson's ratio with increasing pressure. The material displayed thermally advantageous properties for applications at high pressure. The thermal expansion coefficient decreased with increasing Debye temperature.

This means the bonds in the lattice are stronger, which will create better thermal stability. From an optical point of view, pressure could be observed to reduce the bandgap (from 1.95 to 1.12 eV), and it changed from an indirect to a direct bandgap. Furthermore, we noted a higher dielectric response and improved light absorption in the visible–NIR spectrum, implying the tunability of them for solar cell and photonic applications.

Above 15 GPa, a shift from a non-magnetic to a weakly magnetic state emerges magnetically, potentially suggesting an orbital hybridization brought on by pressure and maybe even the start of Stoner-type ferromagnetism. All in all, the properties we saw make $Cs_2AgBiBr_6$ a promising and sustainable option for future optoelectronic and magneto-responsive devices, especially in settings with dynamic or very high pressures.

Ethical Approval:
The authors confirm that it is their original work and has not been submitted elsewhere or published.
Competing interests:
Not applicable
Author's Contribution:
Dr. Abhay Prakash Srivastava prepared the manuscript in an original draft under the supervision of Dr. Sangita Gupta, Dr. Devidutta Maurya, Dr. Sunil Kumar Srivastava, and Dr. Umesh Kumar Pareek.
Funding:
Not applicable
Availability of data and Materials:
Data made available at request.

ORCID

Abhay P. Srivastava, https://orcid.org/0009-0005-9648-0479; **Sangita Gupta,** https://orcid.org/0009-0009-3751-8317

REFERENCES

[1] N. Daem, A. Maho, P. Colson, G. Spronck, C. Malherbe, T.H. Hoang, M.-N. Ghazzal, *et al*., Effect of cations substitution in lead-free double perovskite Cs2AgBiBr6 solar cells, Next Materials, **8**, 100655 (2025). https://doi.org/10.1016/j.nxmate.2025.100655
[2] A.P. Srivastava, and B.K. Pandey, "Enhancing the optoelectronic performance of ABX_3 perovskites (A=MA+/FA+, B=Pb2+, X=I^-/Br^-): A comprehensive first-principles investigation for next generation solar cell technology," International Journal of Modern Physics B, **39**(32), 2550292 (2025). https://doi.org/10.1142/S0217979225502923
[3] Z. Zhang, Q. Sun, Y. Lu, F. Lu, X. Mu, S.-H. Wei, and M. Sui, "Hydrogenated $Cs_2AgBiBr_6$ for significantly improved efficiency of lead-free inorganic double perovskite solar cell," Nat. Commun. **13**, 3397 (2022). https://doi.org/10.1038/s41467-022-31016-w
[4] T.I. Alanazi, "Design and Device Numerical Analysis of Lead-Free $Cs_2AgBiBr_6$ Double Perovskite Solar Cell," Crystals, **13**, 267 (2023). https://doi.org/10.3390/cryst13020267
[5] J. Chen, X. Ma, L. Gong, C. Zhou, J. Chen, Y. Lu, M. Zhou, *et al*., "Improving the performance of lead-free $Cs_2AgBiBr_6$ double perovskite solar cells by passivating Br vacancies," J. Mater. Chem. C, **12**, 14074-14084 (2024). https://doi.org/10.1039/D4TC02339K
[6] S.C. Yadav, J.A.K. Satrughna, and P. M. Shirage, "Investigation of the potential solar cell application of Cs2AgBiBr6 lead-free double perovskite," Journal of Physics and Chemistry of Solids, **181**, 111515 (2023). https://doi.org/10.1016/j.jpcs.2023.111515
[7] D. Maurya, B.K. Pandey, and A.P. Srivastava, "Mechanically robust and optically active $Mg_{80}Ni_{10}Nd_{10}$ metallic glass: first-principles evidence for next-generation optical coatings," Opt. Quant. Electron. **58**, 28 (2026). https://doi.org/10.1007/s11082-025-08615-0
[8] F. Benlakhdar, M.A. Ghebouli, M. Fatmi, B. Ghebouli, S. Alomairy, M.J.A. Abualreish, T. Althagafi, and W. Djerir, "Electronic and optical properties of lead-free $K_2AgSbBr_6$ double perovskite tuned by doping elements Cu^+, Bi^{3+}, and I^-," Sci. Rep. **15**, 40362 (2025). https://doi.org/10.1038/s41598-025-24417-6
[9] A.P. Srivastava, and B.K. Pandey, "DFT-based evaluation of covalent organic frameworks for adsorption, optoelectronic, clean energy storage, and gas sensor applications," Journal of Molecular Modeling, **31**, 302 (2025). https://doi.org/10.1007/s00894-025-06535-0
[10] S. Ullah, T. Alshahrani, F. Khan, and J.F. Rasheed, "Investigating the potential of lead-free Cs2AgBiI6 and Cs2AgBiBr6 double perovskites for photovoltaic applications," Materials Today Communications, **38**, 108514 (2024). https://doi.org/10.1016/j.mtcomm.2024.108514
[11] P. Fan, H.-X. Peng, Z.-H. Zheng, Z.-H. Chen, S.-J. Tan, X.-Y. Chen, Y.-D. Luo, *et al*., "Single-Source Vapor-Deposited $Cs_2AgBiBr_6$ Thin Films for Lead-Free Perovskite Solar Cells," Nanomaterials, **9**, 1760 (2019). https://doi.org/10.3390/nano9121760
[12] S. Choudhary, S. Tomar, D. Kumar, S. Kumar, and A.S. Verma, ЄInvestigations of Lead Free Halides in Sodium Based Double Perovskites Cs2NaBiX6(X=Cl, Br, I): an Ab Initio Study, East European Journal of Physics, (3), 74-80 (2021). https://doi.org/10.26565/2312-4334-2021-3-11

[13] K.-H. Seo, S. Biswas, J. Eun, H. Kim, and J.-H. Bae, "Numerical Study on Overcoming the Light-Harvesting Limitation of Lead-Free $Cs_2AgBiBr_6$ Double Perovskite Solar Cell Using Moth-Eye Broadband Antireflection Layer," Nanomaterials, **13**, 2991 (2023). https://doi.org/10.3390/nano13232991

[14] H. Sabbah, Z.A. Baki, R. Mezher, and J. Arayro, "SCAPS-1D Modeling of Hydrogenated Lead-Free $Cs_2AgBiBr_6$ Double Perovskite Solar Cells with a Remarkable Efficiency of 26.3%," Nanomaterials, 14, 48 (2024). https://doi.org/10.3390/nano14010048

[15] N.K. Nosirova, R.K. Kamilov, M.M. Ibrohimov, L.S. Lepnev, M.O. Astafurov, A.V. Knotko, and A.V.Grigorieva, "Ampoule Synthesis of Na-Doped Complex Bromide $Cs_2AgBiBr_6$ with Double Perovskite Structure," Materials, 18, 1197 (2025). https://doi.org/10.3390/ma18061197

[16] P. Chen, Y. Huang, Z. Shi, X. Chen, and N. Li, "Improving the Catalytic CO_2 Reduction on $Cs_2AgBiBr_6$ by Halide Defect Engineering: A DFT Study," Materials, **14**, 2469 (2021). https://doi.org/10.3390/ma14102469

[17] M. Mehrabian, M. Taleb-Abbasi, and O. Akhavan, "Comparing the performances of Cs_2TiBr_6, $Cs_2AgBiBr_6$, and Cs_2PtI_6 halide compositions in double perovskite photovoltaic devices," Mater Renew Sustain Energy, **14**, 38 (2025). https://doi.org/10.1007/s40243-025-00311-z

[18] A.P. Srivastava, and B.K. Pandey, "Ab initio design of Zr-based bulk metallic glass for high-strength and optical coating applications," Opt. Quant. Electron. **57**, 561 (2025). https://doi.org/10.1007/s11082-025-08467-8

[19] W. Lan, D. Chen, Q. Guo, B. Tian, X. Xie, Y. He, W. Chai, *et al*., "Performance Enhancement of All-Inorganic Carbon-Based $CsPbIBr_2$ Perovskite Solar Cells Using a Moth-Eye Anti-Reflector," Nanomaterials, **11**, 2726 (2021). https://doi.org/10.3390/nano11102726

[20] V. Murgulov, C. Schweinle, M. Daub, H. Hillebrecht, M. Fiederle, V. Dědič, and J. Franc, "Double perovskite $Cs_2AgBiBr_6$ radiation sensor: synthesis and characterization of single crystals," J. Mater. Sci. **57**, 2758–2774 (2022). https://doi.org/10.1007/s10853-021-06847-5

[21] J. Hafner, and G. Kresse, "The Vienna AB-Initio Simulation Program VASP: An Efficient and Versatile Tool for Studying the Structural, Dynamic, and Electronic Properties of Materials," in: *Properties of Complex Inorganic Solids*, edited by A. Gonis, A. Meike, P.E.A. Turchi, (Springer, Boston, MA, 1997). https://doi.org/10.1007/978-1-4615-5943-6_10

[22] A. Kubaib, P.M. Imran, and A.A. Basha," Applications of the Vienna Ab initio simulation package, DFT and molecular interaction studies for investigating the electrochemical stability and solvation performance of non-aqueous NaMF6 electrolytes for sodium-ion batteries," Computational and Theoretical Chemistry, **1217**, 113934 (2022). https://doi.org/10.1016/j.comptc.2022.113934

[23] J.P. Perdew, K. Burke, and M. Ernzerhof, "Generalized Gradient Approximation Made Simple," Phys. Rev. Lett. **77**, 3865 (1996). https://doi.org/10.1103/PhysRevLett.77.3865

[24] É. Brémond, I. Ciofini, and C. Adamo, "Gradient-regulated connection-based correction for the PBE exchange: the PBEtrans model," Molecular Physics, **114**(7–8), 1059–1065 (2016). https://doi.org/10.1080/00268976.2015.1132788

[25] A.P. Srivastava, and B.K. Pandey, "Atomic-Level Design of Doped TiO_2 for Enhanced Lithium Storage: A Density Functional Theory Approach," J. Electrochem. Soc. **172**, 113502 (2025). https://doi.org/10.1149/1945-7111/ae1be1

[26] J. Zhang, J. Attapattu, and J.M. McMahon, "The Pseudopotential Approach within Density-Functional Theory: The Case of Atomic Metallic Hydrogen," Condens. Matter. **5**, 74 (2020). https://doi.org/10.3390/condmat5040074

[27] E. Zafiris, and A.V. Müller, "Electron Beams on the Brillouin Zone: A Cohomological Approach via Sheaves of Fourier Algebras," Universe, **9**, 392 (2023). https://doi.org/10.3390/universe9090392

[28] A.P. Srivastava, and B.K. Pandey, "Pressure-dependent evolution of Bi2Sr2CaCu2O8+δ: DFT insights for high-pressure superconducting applications," Solid State Communications, **404**, 116112 (2025). https://doi.org/10.1016/j.ssc.2025.116112

[29] Z.M. Salikhodzha, G.B. Bairbayeva, R.N. Kassymkhanova, M. Konuhova, K.B. Zhangylyssov, E. Popova, and A.I. Popov, "Density Functional Theory Study of Pressure-Dependent Structural and Electronic Properties of Cubic Zirconium Dioxide," Ceramics, **8**, 41 (2025). https://doi.org/10.3390/ceramics8020041

[30] C.S. Man, and M. Huang, "A Simple Explicit Formula for the Voigt-Reuss-Hill Average of Elastic Polycrystals with Arbitrary Crystal and Texture Symmetries," J. Elast. **105**, 29–48 (2011). https://doi.org/10.1007/s10659-011-9312-y

[31] A.P. Srivastava, and B.K. Pandey, "Analysis of the Structural and Electronic Properties of TiO2 Under Pressure Using Density Functional Theory and Equation of State," Computational Condensed Matter, e01076 (2025). https://doi.org/10.1016/j.cocom.2025.e01076

[32] T.G. Edossa, "Density functional theory study of mechanical, thermal, and thermodynamic properties of zinc-blende CdS and CdSe," Sci. Rep. **15**, 39135 (2025). https://doi.org/10.1038/s41598-025-26168-w

[33] A.P. Srivastava, and B.K. Pandey, "First-principles and equation of state investigation of pressure-tunable structural, mechanical, thermodynamic, and electronic properties of high-reflecting nano-metal oxides: insights into high-performance optoelectronic and energy applications," Appl Nanosci, **15**, 47 (2025). https://doi.org/10.1007/s13204-025-03124-8

[34] A.G. Starikov, M.G. Chegerev, and A.A. Starikova, "A DFT study of electronic structure, magnetic properties and cyclization reaction of [5] helicene derivatives," Computational and Theoretical Chemistry, **1230**, 114369 (2023). https://doi.org/10.1016/j.comptc.2023.114369

[35] M. Adnan, Q. Wang, N. Sohu, S. Du, H. He, Z. Peng, Z. Liu, *et al*., "DFT Investigation of the Structural, Electronic, and Optical Properties of AsTi (B_i)-Phase ZnO under Pressure for Optoelectronic Applications," Materials, **16**, 6981 (2023). https://doi.org/10.3390/ma16216981

[36] A.P. Srivastava, B.K. Pandey, and A. Shanker, P"ressure-Dependent Structural, Mechanical, and Thermal Behavior of $Zr_{50.5}Ti_{4.8}Cu_{19.0}Ni_{11.4}Al_{14.3}$ Bulk Metallic Glass: A DFT and Equation of State Study," Physical Chemistry Research, **14**, e234974 (2025). https://doi.org/10.22036/pcr.2025.552725.2766

[37] T.Y. Ahmed, S.B. Aziz, and E.M.A. Dannoun, "New photocatalytic materials based on alumina with reduced band gap: A DFT approach to study the band structure and optical properties," Heliyon, **10**(5), ne27029 (2024). https://doi.org/10.1016/j.heliyon.2024.e27029

РОЗКРИТТЯ ПЕРЕХОДІВ, ЗУМОВЛЕНИХ ТИСКОМ, У $Cs_2AgBiBr_6$: ВИСНОВКИ ВІД DFT ДЛЯ БЕЗСВИНЦЕВОГО ПЕРОВСКИТУ ДЛЯ СОНЯЧНИХ ЕЛЕМЕНТІВ

Сангіта Гупта[1], Девідутта Маур'я[2], Суніл Кумар Шрівастава[3], Умеш Кумар Парік[3], Абхай П. Шрівастава[4]

[1]Кафедра хімії, Університет Пурніма, Джайпур, Раджастан, Індія

[2]Кафедра фізики, Державний коледж, Баракхал, Санткабірнагар, (UP), Індія

[3]Кафедра прикладних наук, Джайпурський інженерний коледж та дослідницький центр, Джайпур, Раджастан, Індія

[4]Кафедра прикладних наук та гуманітарних наук, Гоельський інститут інженерії та технологій, Лакхнау (UP), Індія

Використовуючи пакет моделювання Віденського Ab initio, ми досліджуємо безсвинцевий подвійний перовскіт $Cs_2AgBiBr_6$. Ми використовували теорію функціоналу густини з перших принципів за тисків до 30 ГПа. Оптимізація структури доводить очевидну кубічну симетрію в навколишньому середовищі. Однак, стиснення, здається, сприяє переходам до фаз з нижчою симетрією, і ми спостерігаємо, що об'єм та модулі Юнга збільшуються, а потім зменшується коефіцієнт Пуассона. Це означає більшу жорсткість, але знижену пластичність. Зроблено висновок, що зі збільшенням температури температура Дебая зростає, а теплове розширення зменшується. Таким чином, передбачається вища температурна стабільність. Електронна заборонена зона стає ще тоншою. Вона охоплює діапазон від 1,95 еВ до 1,12 еВ, що робить її більш-менш прямою, що може підвищити її оптоелектронну зручність використання. Вище 15 ГПа ми спостерігаємо слабкий магнітний момент, очевидно, через гібридизацію Bi-Ag, та вищу густину станів на рівні Фермі. $Cs_2AgBiBr_6$ поєднує ці характеристики, що робить його потенційним матеріалом для фотоелектричних систем з налаштуванням тиску та потенційно для магнітооптоелектронних застосувань.

Ключові слова: *теорія функціоналу густини (DFT); подвійний перовскіт; залежні від тиску властивості; структурний фазовий перехід; оптоелектронні матеріали*